IEEE Access
Multidisciplinary | Rapid Review | Open Access Journal

Received March 28, 2019, accepted May 4, 2019, date of publication May 15, 2019, date of current version May 30, 2019.

*Digital Object Identifier 10.1109/ACCESS.2019.2916952*

# Impact Factor Identification for Switching Overvoltage in an Offshore Wind Farm by Analyzing Multiple Ignition Transients

**JIUJIANG ZHOU, YANLI XIN, WENHU TANG, (Senior Member, IEEE), GANG LIU, AND QINGHUA WU, (Fellow, IEEE)**
School of Electric Power Engineering, South China University of Technology, Guangzhou 510641, China

Corresponding author: Wenhu Tang (wenhutang@scut.edu.cn)

This work was supported in part by the National Natural Science Foundation of China under Grant 51477054 and in part by the Guangzhou Zhiguang Electric Ltd.

**ABSTRACT** This paper investigates the impact factors of switching transient overvoltage (SOV) in an offshore wind farm (OWF) by analyzing multiple ignitions of a vacuum circuit breaker. The statistical features of transient overvoltages, which occur under real switching operation scenarios, are analyzed based on the measurements in a laboratory platform that is built according to the configuration of an actual OWF. Next, an OWF simulation transient model is established considering high-frequency characteristics of circuit breakers, which is verified to be able to calculate the SOV accurately. Based on the developed OWF simulation model, the occurrence mechanism of SOV is discussed in detail by studying characteristics of transient voltage and current during multiple ignitions within a vacuum circuit breaker when it is switched OFF. Then, the key impact factors of switching-OFF induced overvoltage are identified, which include the inter-phase capacitance of cable in a windmill tower, the actual operating capacity of a wind turbine generator, and the single-phase inlet capacitance in terminals of a wind turbine transformer. Finally, the recommended configurations are given for the transient mitigation in an OWF.

**INDEX TERMS** Offshore wind farm, switching overvoltage, multiple ignitions, occurrence mechanism, vacuum circuit breaker.

## I. INTRODUCTION

Due to scheduled energization or de-energization operations as well as unplanned fault-clearing operations, the switching transient overvoltage (SOV) caused by the switching of a vacuum circuit breaker (VCB) is one of common causes that can lead to severe insulation breakdowns of electrical apparatus in an offshore wind farm (OWF) [1]. In particular, this kind of SOV was proven to be able to accelerate transformer failures due to high frequency (HF) induced transients, in which both external ports [2] and internal windings [3], [4] of a transformer were affected. Meanwhile, due to the costs of maintenance and repair in an OWF are much higher than those in an onshore wind farm [5], the requirement of reliability of the equipment in an OWF is also much higher. Therefore, reducing the occurrence probability of severe SOVs and mitigating its damage to the insulation of the system are much necessary and valuable. In order to achieve this purpose, the overvoltage level in different switching conditions should be estimated first, and then the mechanism for the occurrence of SOV during VCB operation process should be understood clearly combined with the physical phenomena. Finally, the impact factors that can influence the characteristics of SOVs should be identified, thus the mitigating methods would be proposed to minimize the damage of the SOVs on the system.

To analyze the occurrence mechanism of SOV in an OWF, several influence factors were investigated, such as prestrikes and reignitions in a VCB [6], length of submarine cable [7], HF characteristics of a VCB [8], and operation scenarios of a VCB [9]. Based on the simulation models developed in [10], the mechanism for the occurrence of SOV under different switching scenarios was discussed by studying the HF interaction in a VCB-transformer-wind turbine generator (WTG) system [11]. Thereinto, the SOV was detected to be most severe, when the VCB was switched off with a low inductive load shortly after energization. This was due to

The associate editor coordinating the review of this manuscript and approving it for publication was Xue Zhou.

that the interruption of inductive current led to HF transient recovery voltages (TRVs), which exceeded the rise rate of dielectric strength (RRDS) and caused multiple ignitions. An on-site test in a real OWF was conducted to study the transient voltage in terminals of wind turbine transformer (WTT) [7], which was caused by the switching-on operations of VCB. The measured transient voltage was below the rated level, while HF components were detected. The prestrikes in the VCB were confirmed to be the main cause of HF voltage, and the configurations of VCB were adjusted to investigate its impact on prestrikes. In addition to the analysis of switching-on SOV in [7], the mechanism for the occurrence of SOV, as induced by switching off a VCB in an OWF, also needs to be further analyzed.

To identify the impact factors of SOV, the methodology for modeling an OWF was studied in [9], which considered both the prestrikes and reignitions when a VCB was switched on and off, respectively. Thereinto, the different physical states were described and their switching logic during the transient was clarified considering HF characteristics of a VCB, including the current chopping level, the HF quenching ability (HFQA), the stray capacitance and the rise rate of dielectric strengthen (RRDS). The RRDS was defined by a linear polynomial in [6], while a more precise RRDS calculation method still needs to be studied due to its importance on simulation results of prestrikes and reignitions.

The impact factors of SOV, as induced by the VCB switching-on in an OWF, were investigated by on-site tests [7]. Thereinto, SOV decreased as the VCB stray capacitance increased, and the decrement of RRDS significantly increased the number of multiple ignitions. Additionally, as the length of the cable between the WTT and the VCB increased, the slope of the TRV decreased. At the same time, the period and amplitude of the oscillations at the beginning of SOV both increased. However, the effect of variations in equipment parameters, such as the inter-phase capacitance (IPC) of cable in a windmill tower, the actual operating capacity (AOC) of WTG, and the single-phase inlet capacitance (SPIC) in terminals of WTT, on SOV still needs to be investigated.

As the essential work of the SOVs effective mitigation in an OWF, the focus of this paper is the mechanism for occurrence of SOVs on the terminal of a WTT and its impact factor identification. A single WTG system in an OWF is established in the laboratory and SOVs on a WTT, caused by the switching of a VCB under four typical switching scenarios, are collected. Then, the features of transient voltages are analyzed, and an OWF model is established, which considers the HF characteristics of key equipment under VCB switching transients. The RRDS calculation method of the established model is improved based on the measured TRV of VCB, and validated by the measured SOV. Employing the improved OWF model, the mechanism for the occurrence of the most severe SOV is investigated, and the impact of practical system configurations on the amplitude and steepness of SOV is identified in detail.

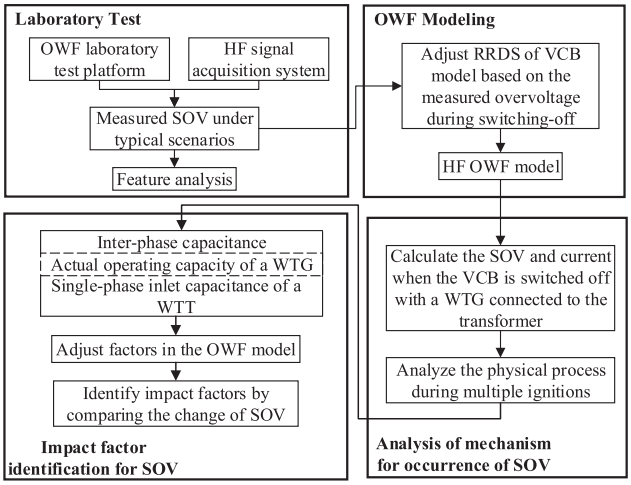


**FIGURE 1.** Research framework for identifying impact factors of SOV.

## II. RESEARCH FRAMEWORK

This research aims to identify the main impact factors of switching overvoltage in an OWF by analyzing multiple ignitions of a VCB. The research framework of this paper is illustrated in Fig. 1.

Laboratory tests based on actual configurations of a single WTG system in an OWF are first conducted to collect transient voltage and current signals. And then, the statistical features of SOV under typical scenarios are analyzed. To investigate the causes of the measured severe SOV, an accurate HF OWF model is established to simulate transient voltages and currents during VCB switching, which is verified by the measured SOV. Next, to identify the impact factors of overvoltage in switching-off operations, the mechanism for its occurrence is investigated with simulations. It includes ignitions in the first opening phase; and virtual current chopping (VCC) with its induced HF SOV. Finally, the impact of three key factors on SOVs from switching-off operations is discussed, including the IPC of cable in a windmill tower, the AOC of WTG, and the SPIC in terminals of WTT.

## III. TEST PLATFORM SETUP

### A. CONFIGURATIONS OF THE LABORATORY TEST PLATFORM

To explore SOVs in an OWF, a single WTG system is constructed in the laboratory based on the topology of Wailuo OWF, located in Zhanjiang, China. Figure 2 shows the topology of the collector system of this OWF, in which the single WTG system in this study is built based on the line diagram in grey. The configurations of the laboratory test platform are in accordance with those in the actual OWF, including the parameters of main equipment, the voltage class of the system, the length of the cable in different locations, the capacity of the WTT and so on, as shown in Fig. 3. Thereinto, $T_G$ is the transformer near WTG. $VCB_G$ represents the VCB located at the bottom of the windmill tower, which is connected to the feeder. $VCB_1$ connects a feeder to a bus and is always closed,

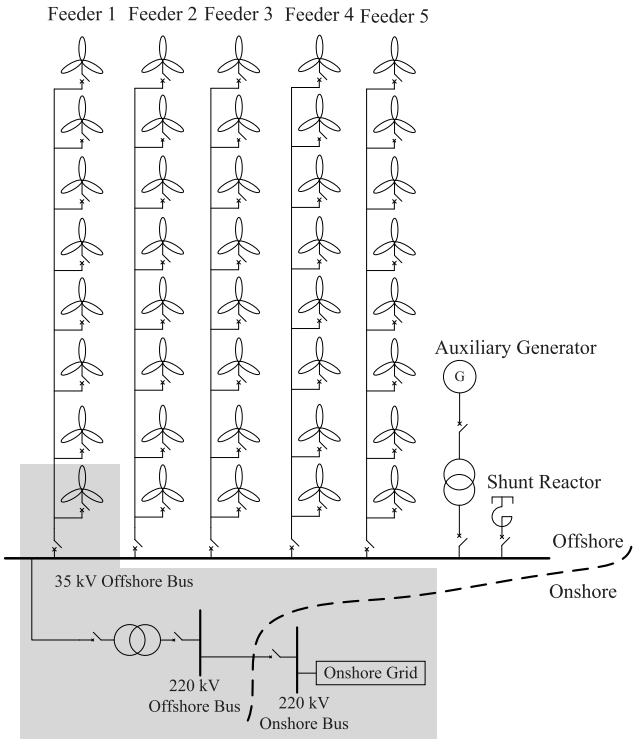


**FIGURE 2.** The topology of wailuo OWF.

as this study mainly investigates the impact of $VCB_G$ switching operations upon $T_G$. The measurements are sampled at three locations, including $MP_1$, $MP_2$, and $MP_3$, as shown in Fig. 3.

The on-site equipment layout is illustrated in Fig. 4. WTG is substituted by a reactor due to a short time-scale for the switching transient study [12]. Its inductance $L_G$ is identified as the equivalent impedance of a running WTG, while its rated capacity is designed as 80% of that of WTT to consider the protection for the reactor from overheating caused by large currents. Thus, the inductance of the reactor $L_G$ is calculated as (1). The actual inductance of the customized reactor in the test is set at 1.0 mH.

$$L_G = \frac{(0.69\ \text{kV})^2}{2\ \text{MVA} \times 0.8} \times \frac{1}{2\pi \times 50} = 0.95\,m\text{H} \qquad (1)$$

For the configuration of the data acquisition system, the transient voltage and current are sampled through a resistance capacitance divider (CD) and a current transformer (CT) respectively, in which their bandwidth and measuring range are sufficient for sampling switching transients based on the parameters of CD and CT in Fig. 3. The input impedances of an oscilloscope interface to the coaxial cable transmitting the CD and CT signals are set at 1 MΩ and 50 Ω respectively, which match the internal impedances of the CD and CT.

The sampling rate of the oscilloscope is set at 40 MHz to ensure the sufficient sampling precision. The sampling length is set at 100 ms, which covers the switching moment and the free oscillation stage. The vertical precision of the

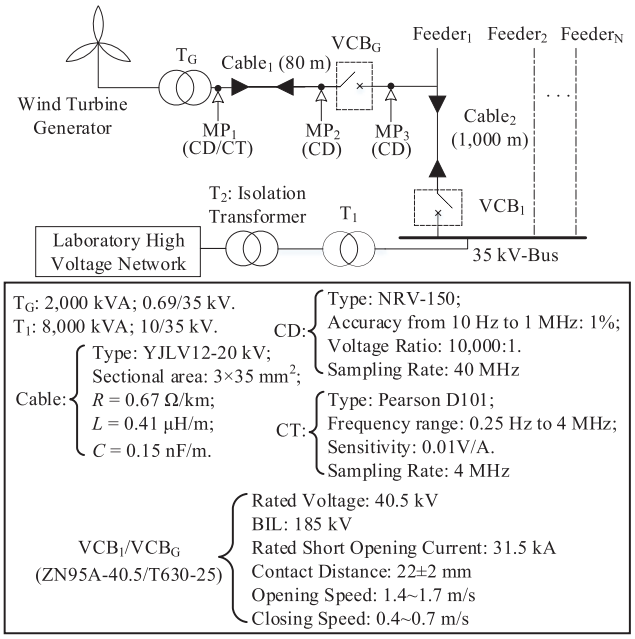


**FIGURE 3.** Topology and equipment parameters of the laboratory test for simulating a single WTG system in OWFs.

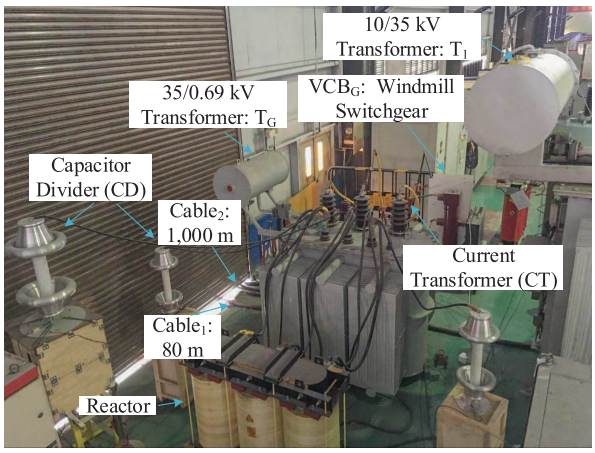


**FIGURE 4.** Equipment layout of the OWF laboratory platform.

oscilloscope is 8 bit, and the vertical measurement range is set at ±150 kV to consider the actual overvoltage measured. Thus, the vertical precision of the recorded signals is $(150\ \text{kV} \times 2)/2^8 = 1.17$ kV, which meets the requirements for conforming the level of SOV and its comparison with rated withstand voltage level of $T_G$.

In addition, the HF signal acquisition scheme of the test system is illustrated in Fig. 5. Here, the ground potential synchronization means that the ground terminals of the CD and CT are both connected to the ground potential of the whole experiment system. The length of the two phase-screened cables, connected to the CD and CT respectively, is set to be equal for reducing the difference of the propagation time. The multi-channel HF transient signals are sampled and stored in the oscilloscope memory synchronously with the same triggering signal of the VCB.

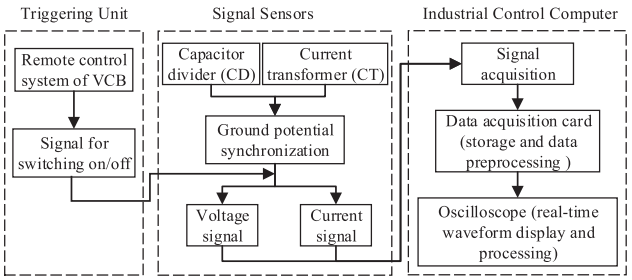


**FIGURE 5.** The data acquisition scheme for HF transient signals.

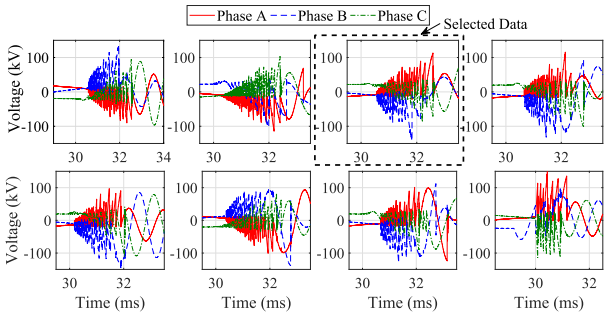


**FIGURE 6.** Measured SOVs with different phase angles of VCB switching operations and the selected one that is presented in section IV.

### B. TECHNICAL DETAILS OF THE CONSTRUCTED PLATFORM

In order to reduce the influence of random factors on the collection of transient signals, the sensors with high precision and high bandwidth, as well as synchronous data sampling, are employed in the test platform. Besides, by analyzing the process of generation and propagation of transients, four random factors are considered in this research.

- The phase angle of the current or voltage when the VCB is switched.
- The residual charge before the VCB is switched on.
- The proximity effect of the high-voltage probe.
- The noise within the measuring circuit.

The countermeasures against these factors are applied in this work, which include:

1) Multiple sets of tests with different phase angles of VCB switching operations were conducted, in which the measured SOVs were detected to be different. To assess the pressure on system insulation, the most severe SOV identified based on time domain characteristics, including the maximum amplitude, reignition times, and voltage steepness, was selected and displayed in Fig. 6.
2) The enclosures of all the components were reliably grounded, and the cable was fully discharged before the system was energized.
3) The distance between the high-voltage probe connected to each phase and any other conductors was set greater than 15 cm, in which the distance was determined in relation to the amplitude of SOV and the interval specified by the specification of the CD. In this way, the effect of the proximity effect on measurements can be greatly reduced, when HF transient signals were generated.
4) The sensors and the main components of the test system were set to share the same earthing point. Moreover, an inductance isolator was added on the ground terminal of the high voltage probe to block grounding currents from flowing through the measuring cable, thus reducing the noise to the measuring circuit.

To illustrate the credibility of laboratory measurements, a comparison of transient voltages in terminals of WTT, between the constructed platform and an actual OWF, is shown in Fig. 7, when the VCB is switched on with the WTG connected. Thereinto, the actual data were collected in Burbo Bank Offshore Wind Farm (BBOWF) owned and operated by DONG Energy and located in the Liverpool bay in the UK [6]. It shows that they share great similarities in regard to major features, such as the duration of transients, the prestrike times and the rise time of prestrike voltage. Therefore, the developed platform can be used to reproduce the SOVs of real operation scenarios in actual OWFs.

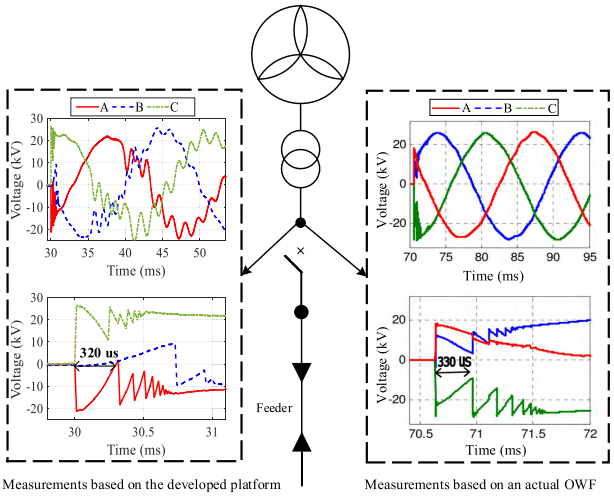


**FIGURE 7.** The comparison of measured transient voltages in terminals of WTT between the laboratory platform and an actual OWF.

In addition, compared with field measurements, the test platform built in this work is reconfigurable for different kinds of tests. In this research, the VCB was operated under different working conditions, and the generated SOVs may damage the component insulation. Such operations are not allowed in an actual OWF for the safe operation of an electrical system. Besides, the VCB can be switched on/off manually many times under different scenarios to assess the most severe SOV that could occur, which is not allowed in an actual OWF. Furthermore, various configurations, such as the length of cable, the movement velocity of VCB contacts, the length of VCB contact gap, and the insulation design of WTT, can be changed on the developed laboratory platform in the following study.

**TABLE 1. Four typical scenarios of switching operations.**

| Scenarios ($S_x$) | Switching operation | WTG |
|---|---|---|
| $S_1$ | On | Disconnected |
| $S_2$ | Off | Disconnected |
| $S_3$ | On | Connected |
| $S_4$ | **Off** | **Connected** |

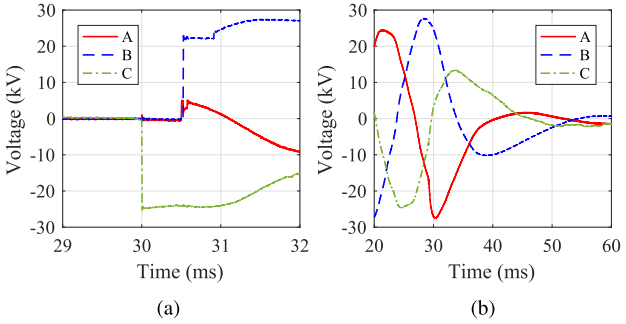


**FIGURE 8. Measured voltage of switching (a) on and (b) off at $MP_1$, when $T_G$ is under the no load condition.**

## IV. STATISTICAL FEATURES OF MEASURED SOV UNDER TYPICAL OPERATION SCENARIOS

Measurements for SOV are taken under four typical operation scenarios, as listed in Table 1. In a real OWF, before a WTG is switched out by $VCB_G$, it is usually first remotely ramped-down until the output power is zero. During this switching off operation, the $T_G$ is still connected to WTG [9], while the $VCB_G$ is switched off. In our tests, the SOVs under the condition that the WTG is in operation, in which the most severe overvoltage may be detected, are measured under $S_4$.

In this research, the experiment results show that when the test system is under $S_1$ or $S_2$, the transient process can be ignored and almost no overvoltage is produced. A few medium frequency oscillations are produced under $S_3$, while the overvoltage that is high in frequency and amplitude is excited under $S_4$. Due to its severe stress being exerted on equipment insulation, the characteristics of SOV, when $VCB_G$ is switched off while the WTG is connected, are discussed in detail in this section.

The transient voltage under scenario $S_1$ at $MP_1$ is shown in Fig. 8(a), in which the voltage with HF or high amplitude is not generated. Prestrikes are not detected during the switching-on process, which is due to the current variation being not significant, when $T_G$ is connected or disconnected under the no load condition. Phase C is first connected and phases A/B are subsequently connected about 0.5 ms later due to the difference in the startup time and the moving speed of the VCB contacts in the three phases. The abrupt change of voltage in all the three phases is not observed under scenario $S_2$, as shown in Fig. 8(b). Shortly after $VCB_G$ is switched off, the voltages decrease to zero gradually due to a small amount of no-load current and the damping effect of $Cable_1$ and $T_G$.

Fig. 9(a) shows the voltages at $MP_1$, which are affected by the prestrikes in $VCB_G$ during energization with the WTG connected. Through analyzing the fluctuation characteristic of the transient voltages in this scenario, it is concluded that although high amplitude overvoltages are not produced, HF voltages in phase A/C are excited at the moment that $VCB_G$ is switched on, while those in phase B appear about 0.7 ms later. The reason could be that the current in phase B still does not pass zero when the VCB is switched on. The HF voltage in phase B is also caused by the prestrikes in phase A/C, in which the HF currents are coupled to phase B due to the inter-phase capacitance coupling in a three-core cable. The main influential factors of the prestrike phenomenon, observed in an actual OWF, were discussed in [7], including the configuration of the collection system, the stray elements in the VCB, and the length of the submarine cable.

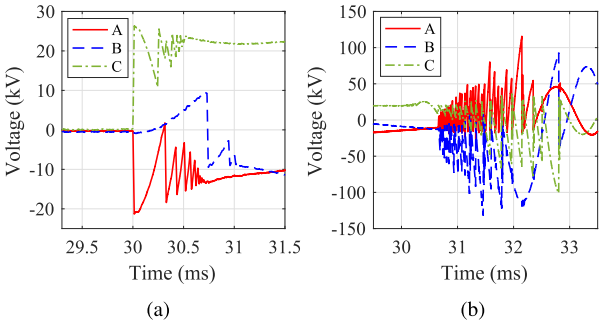


**FIGURE 9. Measured voltage of switching (a) on and (b) off at $MP_1$, when the WTG is connected to $T_G$.**

In scenario $S_4$, the HF transient process lasts about 3 ms, and the measured SOVs in the three phases all rise, as shown in Fig. 9(b), while the distance of $VCB_G$'s contact gap increases throughout this transient process. Compared with the results in Fig. 8(b), the de-energization operation excites more severe SOVs, when the WTG is connected to $T_G$.

In addition, the maximum SOV is excited in phase B, shown in Fig. 9(b), and is relevant to the polarity of the HF current during multiple ignitions. Assuming that $U_T$ is the voltage at $MP_1$ (namely SOV in Fig. 9(b)), $U_S$ is the voltage at the grid side of $VCB_G$ before it is switched off, and the TRV in $VCB_G$ is $U_{VCB}$, their relationship is described as (2).

$$U_T = U_S - U_{VCB} \tag{2}$$

Fig. 9(b) indicates that $U_S$ is 25 kV (near the peak point at 30.1 ms) in phase C, while -12 kV (at 30.6 ms) in phase A and phase B. The polarity of the current in phase C is near zero as the VCB is initially switched off, and changes from negative to positive due to a superimposed power frequency current, which is illustrated in the magnified view of Fig. 10. Subsequently, during multiple ignitions, the HF current in phase A is negative, while the HF current in phase B and phase C are positive (Fig. 10). The polarity of $U_{VCB}$ is the same as that of the HF current. Therefore, the polarity of $U_S$ and $U_{VCB}$ is opposite in phase B, while the same in phase A and phase C. Thus, based on (2), the measured SOV of

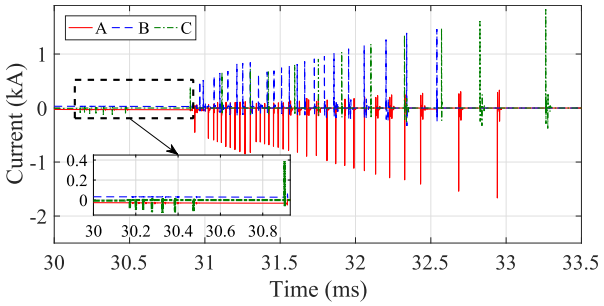


**FIGURE 10.** The polarity of the simulated three-phase current at $MP_1$, when the WTG is connected to $T_G$. The magnified view illustrates the current in phase C when $VCB_G$ is initially switched off.

phase B is higher than that in the other two phases, and reaches about 130 kV.

## V. ACCURATE MODELING OF OFFSHORE WIND FARMS

The test results show that severe HF SOVs are induced on $T_G$, when $VCB_G$ is switched off while WTG is connected. Thus, to reveal the mechanism for the occurrence of SOV in this scenario, and investigate the impact of system configurations on SOV, such as the length of submarine cable [13], the topology of the collector system [14], the setting of reactive power compensation capacity [15], and the arcing characteristic of VCB [16], a HF simulation model for an OWF is built in PSCAD/EMTDC.

In the developed model, the voltage source is replaced by an ideal power grid with an infinite capacity. The parameters of the three-core submarine cable are set according to the actual geometric structure of the cable used in tests. The HF model of $T_G$ is designed with the method in [14], in which the inter-phase stray capacitance and the phase-to-ground capacitance under the HF state are considered. The solution time step in PSCAD is set 0.5 $\mu$s, and it is small enough to calculate SOVs, in which the HF component is around dozens of kilohertz.

For accurate VCB modeling, the chopping current, HFQA, stray capacity of VCB and RRDS are all taken into consideration in this research. The current chopping level mainly depends on the contact material and the load current. It was reported as in the range between 3-8 A under various switching scenarios [17], which is considered as statistically distributed in the established model. HFQA is difficult to be estimated accurately due to the interphase coupling effect in the three-phase cable and that transient inductive currents cannot be changed abruptly. In this research, the typical value of HFQA in a medium voltage system is adopted [17]. Besides, it was found that switching transients were found not sensitive to the stray capacitance of VCB [7], and it is usually adjusted between 10 pF to 60 pF. In this study, the capacitance was set as 40 pF according to the typical value reported in [7].

Due to that RRDS is a key factor for determining whether the recovery voltage exceeds the dielectric strength between contacts during a reignition process [8], [18], a calculation method, which reflects accurate HF characteristics of $VCB_G$ is adopted and described as the followings. The peak points of the measured TRV waveform are piecewisely fitted, which are obtained by taking measurements on the both sides of $VCB_G$, so a piecewise linear RRDS curve is derived. This improvement takes into account the following two factors: (a) the variation of dielectric strength of the vacuum per unit distance caused by multiple ignitions; and (b) the change of separation velocity of the contacts in different positions within its travel range.

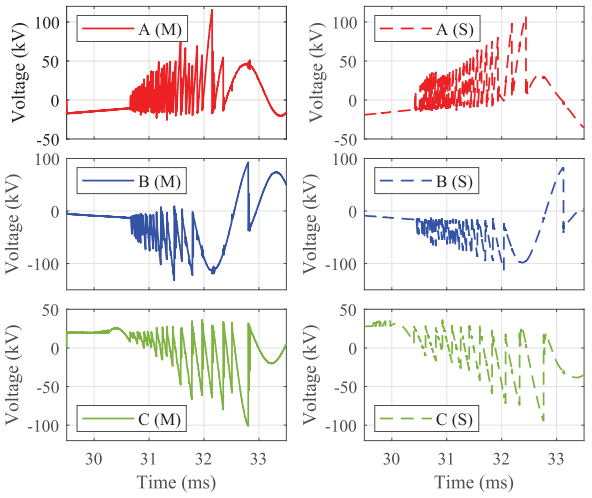


**FIGURE 11.** Comparison between measured and simulated overvoltages at $MP_1$.

**TABLE 2.** Deviations of SOV between measurements and simulations.

| Index | A | B | C |
|---|---|---|---|
| $\delta(U_{max})$ [kV] | 7.3 | 21.0 | **4.0** |
| $\delta(\Delta t)$ [ms] | 0.2 | 0.3 | **0.0** |
| $\delta(N)$ | **1.0** | 3.0 | 4.0 |

The measured and simulated transient voltages at $MP_1$ are compared in Fig. 11. The deviations of SOV between measurements and simulations are listed in Table 2, in which $\delta$ is the absolute difference of statistical indicators for measured and simulated SOVs. The values in bold are the minimum of $\delta$ in the three phases. The results show a good agreement between the measured voltages and simulated voltages in terms of the maximum overvoltage amplitude, the duration of transient process, and the times of repeated ignitions, which are defined as $U_{max}$, $\Delta t$, and $N$, respectively. Thus, the established model, which considers HF characteristics of the main OWF equipment, is validated to be able to reproduce realistic features appearing in real operation scenarios.

## VI. ANALYSIS OF MECHANISM FOR SOV DURING MULTIPLE IGNITIONS OF A VCB

The test results illustrate that severe HF SOV is generated on $T_G$ in $S_4$. The mechanism for the occurrence of this SOV is discussed in this section. The amplitude of this SOV can be suppressed effectively with an arrester, but the HF voltage component cannot be removed. Therefore, to suppress the HF SOV, its mechanism should be discussed first to

investigate which factor may impact the HF components. This discussion is divided into the following two parts: *A*. ignitions in the first opening phase; *B*. virtual current chopping with its induced HF SOV.

### A. IGNITIONS IN THE FIRST OPENING PHASE

When $VCB_G$ is initially switched off, the power frequency current near the zero crossing is chopped first. Fig.12 demonstrates the transient voltage and current during multiple ignitions in the first opening phase. The current in phase C ($I_c$) is chopped firstly at $t_{c1}$, when it is lower than the power-frequency chopping level, as shown in Fig. 12(b). Meanwhile, the TRV in phase C ($V_{VCBc}$) begins to rise. With the increased distance of contacts, $V_{VCBc}$ exceeds the withstand voltage of the contact gap at $t_{c2}$, and the first arc current induced by the vacuum gap breakdown is simultaneously excited. This current lasts about several microseconds and is subsequently interrupted near the zero crossing, when $\left|\frac{di_c}{dt}\right|$ is lower than the HFQA of $VCB_G$ [8].

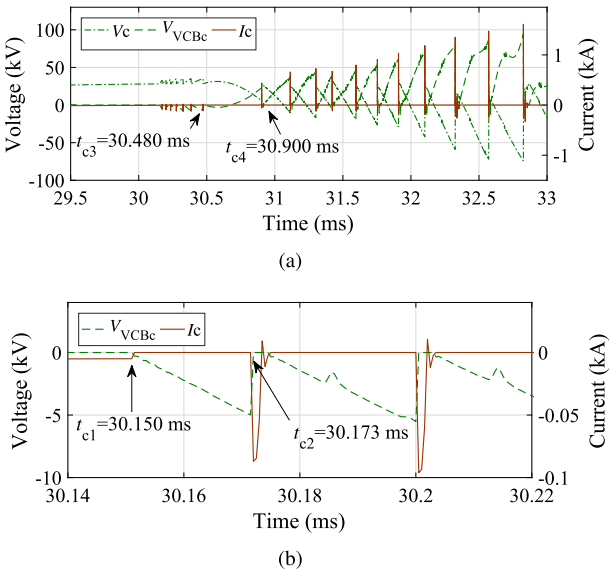


**FIGURE 12.** The simulated transient voltage and current in phase C, when $VCB_G$ is switched off: (a) the HF SOV ($V_c$) and the current ($I_c$) in terminals of $T_G$ and TRV ($V_{VCBc}$) in $VCB_G$ during the whole ignition process; and (b) the magnified view of (a) when the first ignition occurs.

Fig.12(a) shows that the polarity of $I_c$ changes from negative to positive between $t_{c3}$~$t_{c4}$ due to the polarity change of the superimposed power frequency current, and the arcing and arc extinguishing process is repeated during the switching-off process. The multiple ignitions in this first-opening phase are expected to bring about the fact that HF currents are superimposed on the other two phases due to the IPC coupling effect, which accelerates more severe HF SOV.

### B. VIRTUAL CURRENT CHOPPING AND ITS INDUCED SOV

#### 1) HF CURRENT EXCITATION

After the chopping of $I_c$ at $t_{c1}$, the currents in phase A/B ($I_a$ and $I_b$) are chopped at $t_a \approx 30.92$ ms and $t_b \approx 30.95$ ms respectively, as show in Fig. 13(b). Before $t_a$ and $t_b$, $I_a$ and $I_b$

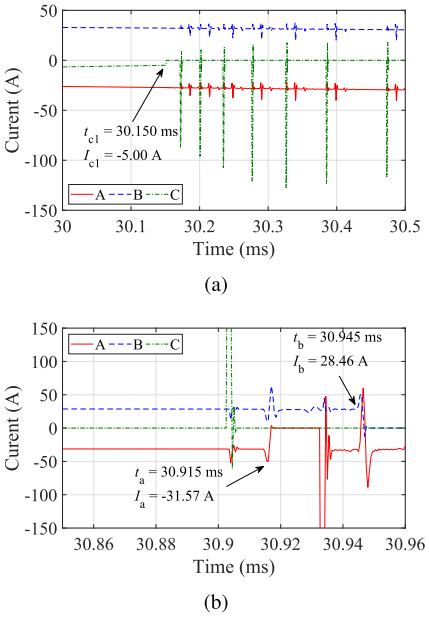


**FIGURE 13.** Simulated transient currents in three phases: (a) currents in three phases between the first ignition in phase C and the first ignition in phase A/B; and (b) power frequency current chopping in phase A and phase B.

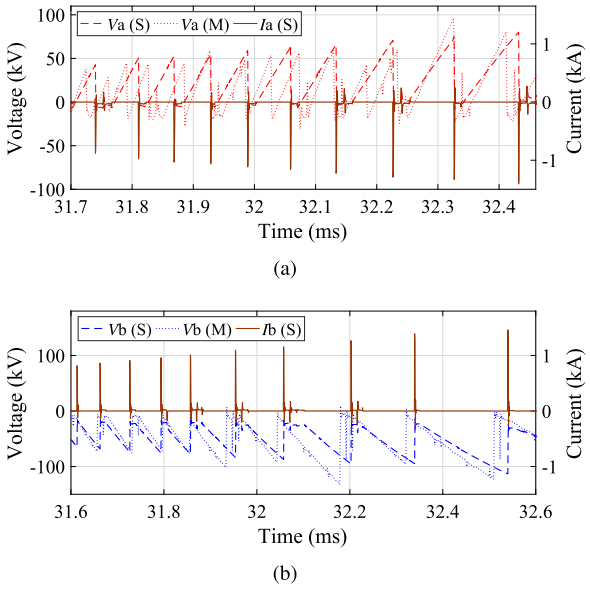


**FIGURE 14.** Simulated SOV *V*(S) and current *I*(S) as well as measured SOV *V*(M) in terminals of $T_G$, when $VCB_G$ is switched off: (a) Phase A; and (b) Phase B.

are both superimposed with HF components coupled from phase C owing to the IPC coupling effect of the three-core cable, which can be confirmed in Fig.13(a) As the steepness of the superimposed HF currents is larger than the HFQA of $VCB_G$ from $t_{c1}$ to $t_a$ and from $t_{c1}$ to $t_b$ in phase A/B, both $I_a$ and $I_b$ cannot be chopped until $t_a$ and $t_b$ respectively, and $I_a$ and $I_b$ are chopped at 31.57 A and 28.46 A respectively, as shown in Fig. 13(b). After the first current chopping in phase A/B, the arc currents in these two phases rise, exceeding 1 kA (Fig. 14) due to an increase of TRVs

**TABLE 3. Calculation of voltage steepness for phases A and B (based on Fig. 14).**

| Phase | Steepness(kV/$\mu$s) | Ignition sequence number | | | | | | | | | |
|---|---|---|---|---|---|---|---|---|---|---|---|
| | | 1 | 2 | 3 | 4 | 5 | 6 | 7 | 8 | 9 | 10 |
| A | $\lvert dU/dt\rvert$ | 69.46 | 70.67 | 73.83 | 77.19 | 79.62 | 80.16 | 83.52 | 87.55 | 92.18 | 94.71 |
| | $i/C_o$ | 58.66 | 64.98 | 66.22 | 70.96 | 71.41 | 77.38 | 78.31 | 82.62 | 85.32 | 89.77 |
| | $\Delta$ | **10.80** | 5.69 | 7.61 | 6.23 | 8.21 | **2.78** | 5.21 | 4.93 | 6.86 | 4.94 |
| B | $\lvert dU/dt\rvert$ | 77.31 | 79.56 | 81.45 | 84.36 | 87.24 | 94.63 | 97.16 | 101.99 | 102.48 | 106.59 |
| | $i/C_o$ | 54.35 | 57.51 | 60.82 | 63.94 | 67.31 | 73.17 | 77.12 | 84.48 | 92.73 | 97.43 |
| | $\Delta$ | **22.96** | 22.05 | 20.63 | 20.42 | 19.93 | 21.46 | 20.04 | 17.51 | 9.75 | **9.16** |

in $VCB_G$. In addition, SOVs in phase A/B also rise during these multiple ignitions. Therefore, the impact of $Cable_1$'s IPC on SOV should be investigated, considering its effect on the HF current coupling between the three phases of the three-core cable.

### 2) STEEPNESS CALCULATION OF SOV INDUCED BY VCC

With the distance increase of the VCB's contact gap, the breakdown voltage induced by each ignition increases, as does the HF coupling current. Due to the limitation of the HFQA of VCB, the HF current is interrupted every time those electric arc extinguish during the multiple ignitions (Fig. 14).

This kind chopping of HF coupling current, also known as VCC, leads to an independent oscillating circuit in $Cable_1$, $T_G$ and WTG in each phase. Meanwhile, the steepness of the induced SOV can be calculated by (3) [19].

$$\left|dU/dt\right| = \left|i/C\right| \tag{3}$$

where $U$ and $i$ are the single-phase voltage and current in terminals of $T_G$ respectively, $C$ is the total phase-to-ground capacitance at the load side of $VCB_G$, which includes the single-phase capacitance of $Cable_1$ and the SPIC in terminals of $T_G$, as labeled with $C_C$ and $C_T$ respectively. According to the parameters of cable (Fig. 3) and the recommended value in [14], $C = C_C + C_T = 0.15\ \text{nF/m} \times 80\ \text{m} + 3\ \text{nF} = 15\ \text{nF}$.

To verify the relationship of (3), namely whether the impact of the HF current and the total phase-to-ground capacitance on the steepness of SOV is in accordance with the relationship in (3), the SOV and HF current in phase A/B during ten ignitions are calculated in Fig. 14. The statistical results of $\left|dU/dt\right|$ and $\left|i/C\right|$, when the breakdown occurs, are listed (Table 3). Here, the difference between $\left|dU/dt\right|$ and $\left|i/C\right|$, defined as $\Delta$, are (2.78~10.8) kV/$\mu s$ and (9.16~22.96) kV/$\mu s$ in phase A/B respectively. It is also deduced from Table 3 that the variations of $\left|dU/dt\right|$ and $\left|i/C\right|$ share the same tendency in phase A/B, as the $VCB_G$'s contact gap increases. The above discussion indicates that $i$ and $C$ are the two main impact factors on SOV steepness.

In a real OWF, the AOC of WTG is considered to be a factor that may change the HF current $i$ due to that the output voltage of WTG is constant. Then based on the definition of capacitance $C$, it consists of the capacitance of $Cable_1$ and terminals of $T_G$, in which the SPIC of $T_G$ is considered to be adjustable to investigate its impact on SOV due to that the length of $Cable_1$ is usually fixed by the height of windmill tower. Therefore, the identification of these three factors needs to be discussed further.

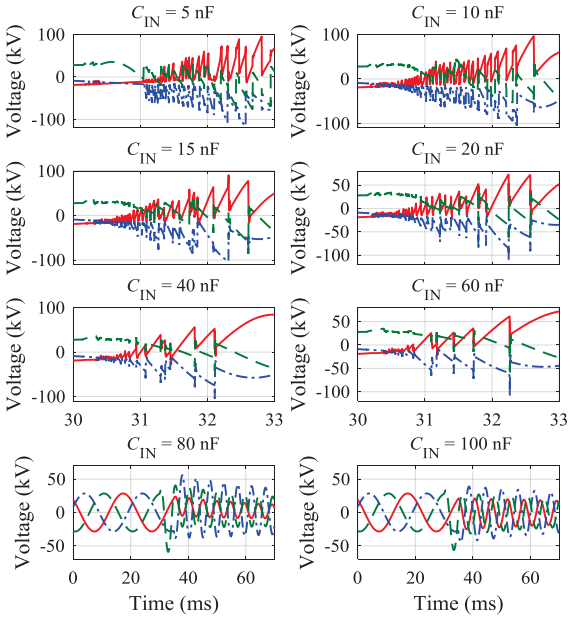


**FIGURE 15. Simulated SOVs when $C_{IN}$ increases from 5 nF to 100 nF.**

## VII. IMPACT FACTORS OF OVERVOLTAGE INDUCED BY VCB SWITCHING-OFF

Based on the mechanism analysis of SOV generation during $VCB_G$ switching-off in section VI, the impact of three factors, i.e. IPC of $Cable_1$, AOC of WTG, and SPIC in terminals of $T_G$ on SOV, are discussed in this section.

### A. THE IPC OF CABLE1

Firstly, the impact of the IPC of $Cable_1$ on SOV induced by $VCB_G$ switching-off is investigated. Fig. 15 shows SOVs when the IPC varies from 5 nF to 100 nF. Here, the IPC of $Cable_1$ is defined as $C_{IN}$. Additionally, the range setting of $C_{IN}$ takes into account the inter-phase shielding and insulation layers of $Cable_1$ and refers to the single-phase-to-ground capacitance.

When $C_{IN}$ increases from 5 nF to 10 nF, more HF voltage, which is small in amplitude, is excited within 1 ms upon $VCB_G$ is switched off. Meanwhile, the amplitude of SOV during the whole transient process is almost invariant. When $C_{IN}$ increases from 10 nF to 60 nF, the amplitude and steepness of

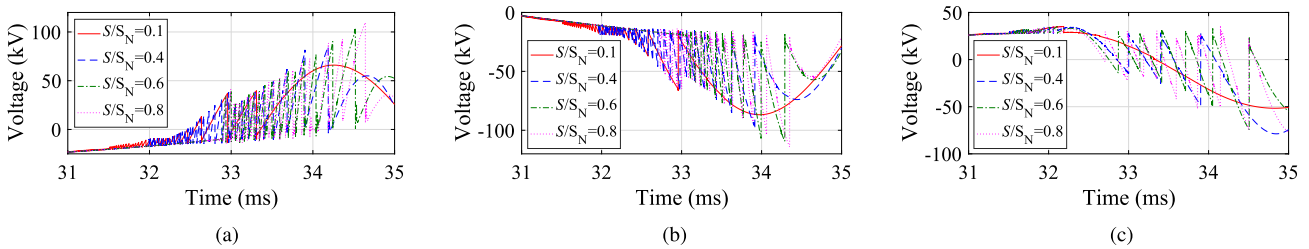


**FIGURE 16.** Simulated SOVs in three phases during multiple ignitions, when the AOC of WTG is changed. (a) Phase A. (b) Phase B. (c) Phase C.

SOV as well as the number of multiple ignitions all decrease. It is due to the decrease of the rise rate of TRV in $VCB_G$, which is caused by the decrease of the resonance frequency of the $Cable_1$-$T_G$-WTG system when $C_{IN}$ increases.

When $C_{IN}$ is located in the range of 60 nF to 100 nF, abrupt changes of voltage disappear, and meanwhile the duration of low frequency oscillations obviously increases. In this case, the rise rate of TRV and the times of multiple ignitions both decrease owing to the IPC increment in this range. When $C_{IN}$ equals 80 nF, the transient process with ignitions is suppressed completely and the VCB is switched off within a few milliseconds, while the duration of low frequency oscillations increases prominently.

According to the above comparison, the setting of IPC should follow the principle that HF SOVs during switching transient are mitigated most effectively, and meanwhile the duration of low frequency oscillations is reduced. In addition, the IPC should be (a) treated as one of electrical parameters for a submarine cable in its design stage and (b) configured by adjusting geometrical structure parameters.

### B. THE AOC OF WTG

The AOC of WTG is adjusted to study its impact on SOV induced by $VCB_G$ switching-off at $MP_1$. The ratio of AOC ($S$) of WTG to the rated capacity ($S_N$) of WTG, defined as $S/S_N$, is set to the following four values: 0.1, 0.4, 0.6 and 0.8. The comparison of SOV in the three phases during multiple ignitions is shown in Fig. 16. The statistical parameters, including the maximum, steepness, and times of abrupt changes in voltage, all decrease, while $S/S_N$ is decreased from 0.8 to 0.1. Meanwhile, the times of voltage fluctuations with a small range during the primary stage of contact separation increases as $S/S_N$ decreases, which can be ignored for insulation protection due to its low amplitudes.

The absolute values of the maximum amplitude and maximum steepness of SOV during multiple ignitions, defined as $|U_{max}|$ and $|dU/dt|_{max}$ respectively, are both calculated (Table 4). When $S/S_N$ equals 0.8, $|U_{max}|$ and $|dU/dt|_{max}$ are close to those when WTG is under the full load, as shown in Fig. 9(b). When $S/S_N$ is reduced to 0.1, they both have a significant decrease compared with those when $S/S_N$ is 0.4. When $S/S_N$ is equal to 0 (namely $T_G$ is in the no-load condition), the voltages at $MP_1$ are shown in Fig. 8(b), in which no SOV is observed.

**TABLE 4.** The maximum and steepness of SOV for changed AOC.

| Parameters | $S/S_N$ | Phase | | |
|---|---|---|---|---|
| | | A | B | C |
| $\|U_{max}\|$ [kV] | 0.1 | 39.7 | 66.3 | 35.2 |
| | 0.4 | 84.8 | 97.6 | 47.6 |
| | 0.6 | 102 | 109 | 74.2 |
| | **0.8** | **110** | **115** | **75.0** |
| $\|dU/dt\|_{max}$ [kV/$\mu$s] | 0.1 | 50.7 | 81.5 | 7.4 |
| | 0.4 | 90.0 | 115 | 77.4 |
| | 0.6 | 98.5 | 127.3 | 90.6 |
| | **0.8** | **103** | **135.6** | **98.0** |

It can be summarized that the amplitude and steepness of SOV both decrease when $S/S_N$ decreases. The maximum chopping overvoltage $U_{ch}$ during multiple ignitions in the VCB can be calculated using (4).

$$U_{ch} = \sqrt{\frac{L}{C} \cdot I_{ch}^2 + U_m^2} \tag{4}$$

$L$ and $C$ are the inductance and the capacitance of the cable-transformer-WTG system on the load side of $VCB_G$, respectively. $I_{ch}$ is the HF chopping current, and $U_m$ is the peak of the single-phase power frequency voltage. It can be deduced that when WTG operates with the full power, the inductive current of system is the maximum and $U_{ch}$ also reaches its maximum. Equation (3) also indicates that the steepness of SOV is affected by the inductive current, which is relevant to the level of AOC of WTG. The statistics (Table 4) verify that the voltage steepness drops with the decrease of $S/S_N$.

According to the IEEE standard C57.12.00 [20], in a 35 kV system, the recommended values of the basic lightning impulse insulation level (BIL) and the basic switching impulse insulation level (BSL) of a transformer are 125 kV and 104 kV respectively. Thus, the phase-to-ground BSL is 85 kV ($104\ \text{kV} \times \sqrt{2}/\sqrt{3} = 85\ \text{kV}$). The front time of SOV induced by multiple ignitions of the VCB ranges from 10 $\mu$ s to 100 $\mu s$ according to the investigation reported in [21], so the rated withstand steepness of the transformer for switching impulses is set as 1.02 kV/$\mu s$ to 10.2 kV/$\mu s$. By comparing the SOV (Table 4) with the mentioned BSL, severe damage to the system insulation can be induced under the scenario $S_4$. Therefore, WTG is suggested to be shut down first before switching off $VCB_G$ to avoid this kind of stress.

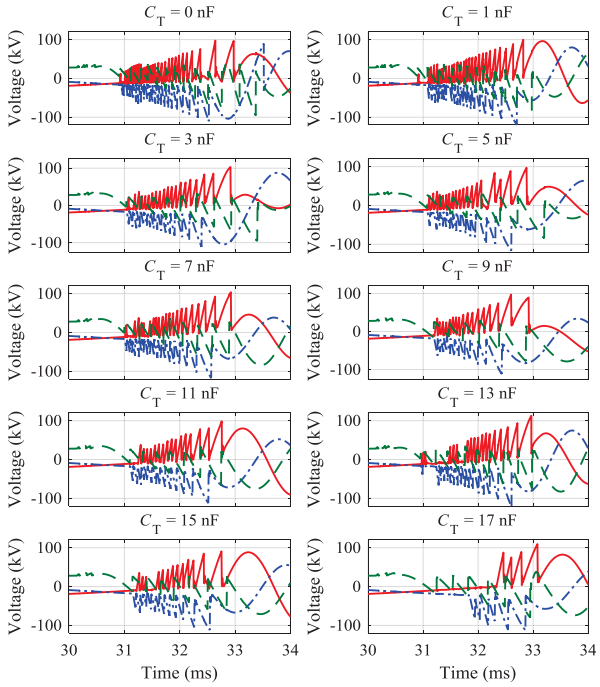


**FIGURE 17.** Simulated SOVs in three phases during multiple ignitions, when the SPIC of $T_G$ changes from 0 nF to 17 nF.

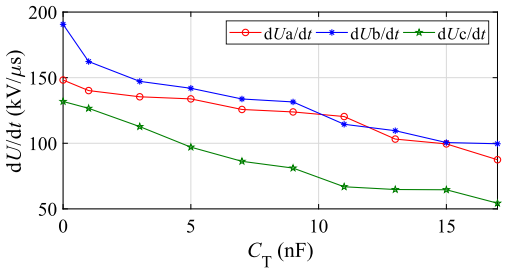


**FIGURE 18.** The calculated maximum rise rate of SOV in three phases for variations in the SPIC.

### C. THE SPIC OF WTT

The SPIC of $T_G$ is dependent upon the material and the geometric structure of transformer winding. It is more significant when voltage surges are exerted on the transformer. Based on the reported typical capacitances of a core-type transformer with different capacities in [22], when it suffers from switching surges, the SPIC of $T_G$ ($C_T$) varies from 0 nF to 17 nF. In this section, SPIC is adjusted in this range to investigate its impact on the steepness of SOV caused by switching-off operations.

SOVs in terminals of $T_G$, when $C_T$ increases from 0 nF with a fixed interval (2 nF), is calculated in Fig. 17. Thereinto, the maximum SOV ($U_{max}$) varies in a narrow range, while the number of repeated ignitions ($N$) decreases, as $C_T$ increases from 0 nF to 17 nF. The maximum steepness of SOV ($|dU/dt|_{max}$) in the three phases also decreases with the increment of $C_T$ (Fig. 18). Though the decreasing range of $|dU/dt|_{max}$ in the three phases varies when $C_T$ rises from 0 nF to 17 nF, $|dU/dt|_{max}$ continuously drops.

The reason for this phenomenon is that the rise of $C_T$ increases the oscillating period and reduces the rise rate of recovery voltage on the load side of $VCB_G$. When an ignition is cleared, the $Cable_1$-$T_G$-WTG system is disconnected to the feeder. When $C_T$ rises, the resonant frequency of this system, defined as $f_0$, is reduced according to (5), as discussed in [23]. Due to this frequency reduction, the steepness of SOV also drops, thus causing the rise rate of TRV in $VCB_G$ to fall, and the number of multiple ignitions ($N$) to decrease.

$$f_0 = \frac{1}{2\pi\sqrt{LC}} \tag{5}$$

In summary, under the configuration in this study, the increase of SPIC of WTT reduces the steepness of SOV. Therefore, adjusting SPIC can be considered for the mitigation of HF SOV. Moreover, several protection devices using additional capacitance snubbers in terminals of transformer are investigated in [24]. Finally, as adjusting SPIC cannot mitigate the amplitude of SOV, the setting of the SPIC should be coordinated with that of the parameters of other protection devices for effective SOV suppression.

## VIII. APPLICATION OF THE IMPACT IDENTIFICATION ON AN ACTUAL OWF

In this section, a practical case study is presented to show how the investigation of this work can be applied to solve practical problems in the field. An accident of insulation breakdown of a transformer in Wailuo OWF was reported during its trial operation stage in May 2018. The partial circuit diagram of the OWF, when the accident happened, is shown in Fig. 19 (a). A brief description of the accident is given as follows.

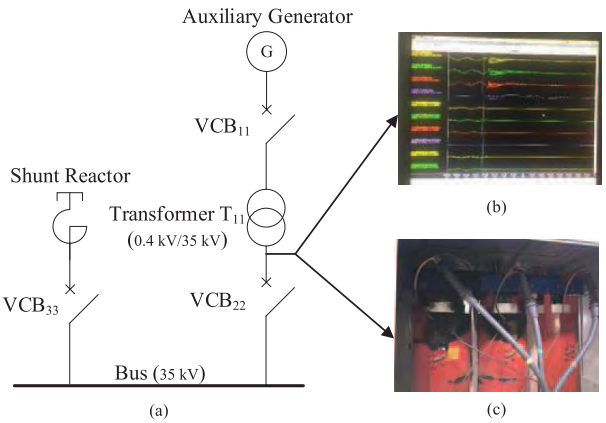


**FIGURE 19.** An actual case of insulation breakdown of a transformer in an OWF. (a) The partial circuit diagram of the actual OWF when the accident happened. (b) The recorded SOVs in the terminal of transformer when $VCB_{22}$ is switched off. (c) The breakdown of transformer insulation due to the severe SOVs.

First, an auxiliary diesel generator was started with the full power to supply a shunt reactor, as well as the heating and dehumidification equipment of the collector system of the OWF. The switchgears $VCB_{11}$ and $VCB_{22}$ were switched on respectively, and the voltage and current at every location of the system were detected to be in a normal condition.

Then the shunt reactor was energized with $VCB_{33}$ switching on, as the reactive load of the auxiliary generator. Finally, due to the improper setting of relay protection, $VCB_{22}$ was forcedly switched off, while severe SOVs were induced in the terminals of $T_{11}$, as shown in Fig. 19 (b). Meanwhile the insulation of T11 was broken and blackened, as shown in Fig. 19 (c).

Through comparing both the topology and the SOVs between the actual OWF and the developed experimental platform, which can be compared between Fig. 19 (a) and Fig. 3 as well as Fig. 19 (b) and Fig. 9 (b), the accident caused by $VCB_{22}$ switching off shares similarities with the switching operations under scenario $S_4$, as discussed in section IV. Therefore, based on the occurrence mechanism analysis in section VI, the virtual current chopping within $VCB_{22}$ is revealed as the primary cause for the severe SOVs. Considering the impact factors identified in this research, two feasible solutions are proposed as follows.

- Add another auxiliary diesel generator connected to the bus for maintaining the whole output, while reducing the actual output of each generator.
- Add RC snubbers in three phases of terminals of the transformer $T_{11}$.

The first scheme is to suppress the amplitude of SOVs by reducing the AOC of each generator. The second one is to mitigate the steepness of SOVs by increasing the SPIC of each phase in terminals of the transformer. Both the two solutions are derived from the impact factor identification process investigated in this research. To test the effect of the proposed solutions, transient voltages under the same VCB switching scenario of this accident were simulated in PSCAD/EMTDC. The comparison results before and after applying the proposed solutions are shown in Fig. 20. It shows that original severe SOVs are suppressed effectively, after the proposed solutions are adopted, in which the amplitude, steepness, and reignition times are all reduced significantly.

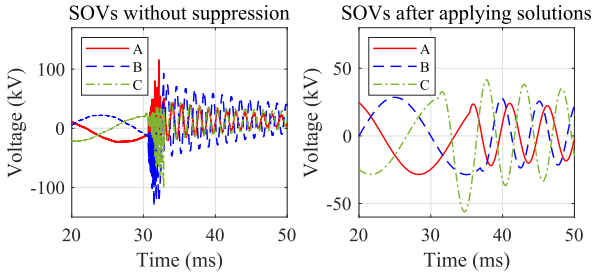


**FIGURE 20. The comparison of simulated transient voltages before and after applying the proposed solutions.**

## IX. CONCLUSION

The main novelty of this work include two aspects. First, based on a laboratory test platform which can simulate realistic operation scenarios of OWFs, the occurrence mechanism of SOVs is revealed through analyzing variation characteristics of the transient voltages in the VCB and the terminals of WTT, as well as the transient currents. The results demonstrate that the VCC during multiple ignitions is the main cause of SOV. Second, three key impact factors that influence SOVs are identified, including the IPC of a cable in a windmill tower, the AOC of WTG, and the SPIC in terminals of WTT. It is worth mentioning that the test results in this work are obtained based on the constructed experimental platform, which are applicable only to those applications with similar settings of equipment and voltage/power as the experimental platform.

It is detected that when an inductive load, such as WTG or shunt reactor, is directly disconnected from the collect system by a VCB in an OWF, severe SOVs are very likely to occur and result in serious damage to main components. To mitigate this kind of severe SOVs, several feasible recommendations are proposed based on the adjustment of the three identified impact factors. Thereinto, the IPC of cable in a windmill tower can be increased to suppress both the amplitude and frequency of SOVs effectively; the AOC of WTG can be reduced to limit the amplitude of SOVs, and if possible it should be shut down first before switching off a VCB for effective overvoltage suppression effect; increasing the SPIC in terminals of WTT is discovered to be an effective method to mitigate the steepness of SOVs, and it can be realized by installing RC snubbers in terminals of WTT in an OWF. These technical solutions are applied on a practical case in an actual OWF, and the severe SOVs are suppressed effectively with the proposed solutions, as presented in section VIII.

In addition, based on the recorded experimental results, an improvement on the WTG model, which includes LC filters and reproduces the frequency range of VCB switching transients, should be carried out in future work to accurately calculate SOVs in simulations. Another issue that needs to be noted is that more severe inter-phase or inter-winding overvoltage inside the transformer in an OWF could be induced by the SOV in terminals of WTT, which is due to the difference of surge impedance of the power collection system between OWFs and onshore wind farms. Therefore, the research on the internal overvoltage of the transformer in an OWF is deserved to be studied in the future.

## REFERENCES

[1] T. Abdulahovic, "Analysis of high-frequency electrical transients in offshore wind parks," Ph.D. dissertation, Chalmers Univ. Technol., Gothenburg, Sweden, 2011.

[2] M. Popov, R. P. P. Smeets, L. V. D. Sluis, H. D. Herdt, and J. Declercq, "Experimental and theoretical analysis of vacuum circuit breaker prestrike effect on a transformer," *IEEE Trans. Power Del.*, vol. 24, no. 3, pp. 1266–1274, Jul. 2009.

[3] D. D. Shipp, T. J. Dionise, V. Lorch, and B. G. MacFarlane, "Transformer failure due to circuit-breaker-induced switching transients," *IEEE Trans. Ind. Appl.*, vol. 47, no. 2, pp. 707–718, Mar. 2011.

[4] A. Theocharis, M. Popov, R. Seibold, S. Voss, and M. Eiselt, "Analysis of switching effects of vacuum circuit breaker on dry-type foil-winding transformers validated by experiments," *IEEE Trans. Power Del.*, vol. 30, no. 1, pp. 351–359, Feb. 2015.

[5] R. L. King, "Electrical transmission systems for large offshore windfarms," Ph.D. dissertation, Dept. Elect. Eng., Cardiff Univ., Cardiff, U.K., 2011.

[6] S. M. Ghafourian, "Switching transients in large offshore wind farms: System components modeling," Ph.D. dissertation, Univ. Manchester, Manchester, U.K., 2015.

[7] S. M. Ghafourian, I. Arana, J. Holbøll, T. Sørensen, M. Popov, and V. Terzija, "General analysis of vacuum circuit breaker switching overvoltages in offshore wind farms," *IEEE Trans. Power Del.*, vol. 31, no. 5, pp. 2351–2359, Oct. 2016.
[8] T. Abdulahovic, T. Thiringer, M. Reza, and H. Breder, "Vacuum circuit-breaker parameter calculation and modelling for power system transient studies," *IEEE Trans. Power Del.*, vol. 32, no. 3, pp. 1165–1172, Jun. 2017.
[9] I. A. Aristi, "Switching overvoltages in offshore wind power grids," Ph.D. dissertation, Dept. Elect. Eng., Tech. Univ. Denmark, Kongens Lyngby, Denmark, 2011.
[10] B. Badrzadeh, M. Høgdahl, and E. Isabegovic, "Transients in wind power plants—part I: Modeling methodology and validation," *IEEE Trans. Ind. Appl.*, vol. 48, no. 2, pp. 794–807, Mar./Apr. 2012.
[11] B. Badrzadeh, M. H. Zamastil, N. K. Singh, H. Breder, K. Srivastava, and M. Reza, "Transients in wind power plants–Part II: Case studies," *IEEE Trans. Ind. Appl.*, vol. 48, no. 5, pp. 1628–1638, Sep./Oct. 2012.
[12] M. Reza and H. Breder, "Cable system transient study: Vindforsk V-110: Experiments with switching transients and their mitigation in a windpower collection grid scale model," ABB Corp., Zurich, Switzerland, Tech. Rep., Jan. 2009.
[13] Y. L. Xin, W. H. Tang, L. Luan, G. Y. Chen, and Q. H. Wu, "Overvoltage protection on high-frequency switching transients in large offshore wind farms," in *Proc. IEEE Power Energy Soc. Gen. Meeting (PESGM)*, Jul. 2016, pp. 1–5.
[14] Y. L. Xin, B. Liu, W. H. Tang, and Q. H. Wu, "Modeling and mitigation for high frequency switching transients due to energization in offshore wind farms," *Energies*, vol. 9, no. 12, pp. 1044–1059, Dec. 2016.
[15] H. A. Hamid, N. Harid, M. A. Haddad, and H. Griffiths, "Modelling of a 400-kV MSCDN reactor for computation of voltage and field distributions during switching transients," *IEEE Access*, vol. 6, pp. 36247–36255, 2018.
[16] J. Yuan, W. Jianwen, and J. Bowen, "Reignition after interruption of intermediate-frequency vacuum arc in aircraft power system," *IEEE Access*, vol. 6, pp. 8649–8656, 2018.
[17] C. L. Bak *et al.*, "Vacuum circuit breaker modelling for the assessment of transient recovery voltages: Application to various network configurations," *Electr. Power Syst. Res.*, vol. 156, pp. 35–43, Mar. 2018.
[18] M. T. Glinkowski, M. R. Gutierrez, and D. Braun, "Voltage escalation and reignition behavior of vacuum generator circuit breakers during load shedding," *IEEE Trans. Power Del.*, vol. 12, no. 1, pp. 219–226, Jan. 1997.
[19] Y. G. Guan, Q. W. Tang, W. D. Liu, and G. Z. Xu, "Overvoltage mechanism of switching off shunt reactors for 40.5 kV vacuum circuit breakers," *Proc. CSEE*, vol. 32, no. 33, pp. 124–132, Nov. 2012.
[20] *IEEE Standard for General Requirements for Liquid-Immersed Distribution, Power, and Regulating Transformers*, IEEE Standard C57.12.00, 2015.
[21] S. V. Kulkarni and S. A. Khaparde, *Transformer Engineering: Design and Practice*. New York, NY, USA: Marcel Dekker, 2004.
[22] J. C. Das, "Surges transferred through transformers," in *Proc. Annu. Pulp Paper Ind. Tech. Conf.*, Jun. 2002, pp. 139–147.
[23] A. Working Group, "Guide for application of IEC 62271-100 and IEC 62271-1, Part 2: Making and breaking tests," Int. Council Large Electr. Syst., Paris, France, Tech. Rep., 2006, vol. 305.
[24] P. E. Sutherland, M. E. Valdes, and G. H. Fox, "Snubber design for transformer protection," *IEEE Trans. Ind. Appl.*, vol. 52, no. 1, pp. 692–700, Jan./Feb. 2016.

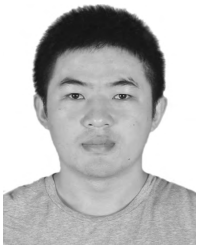

**JIUJIANG ZHOU** received the B.Sc. degree in electrical engineering from Huaqiao University, Xiamen, China, in 2012, and the M.S. degree in electronics and communication engineering from Hunan University, Changsha, China, in 2015. He is currently pursuing the Ph.D. degree with the South China University of Technology, China. His major research interests include transient analysis and overvoltage suppression of power systems.

**YANLI XIN** received the B.Sc. degree in electrical engineering from the Jiangxi University of Technology, China, in 2012. She is currently pursuing the Ph.D. degree in electrical engineering with the South China University of Technology, China. Her research interests include electromagnetic transient modeling of power systems and resilience modeling of power grid.

**WENHU TANG** (M'05–SM'13) received the B.Sc. and M.Sc. degrees in electrical engineering from the Huazhong University of Science and Technology, Wuhan, China, in 1996 and 2000, respectively, and the Ph.D. degree in electrical engineering from The University of Liverpool, Liverpool, U.K., in 2004. He was a Postdoctoral Research Associate and subsequently a Lecturer with The University of Liverpool, from 2004 to 2013. He is currently a Distinguished Professor and the Dean of the School of Electric Power Engineering, South China University of Technology, Guangzhou, China. He has authored or coauthored more than 100 research papers, including 40 journal papers and one Springer research monograph. His research interests include power systems risk assessment, renewable energy integration in power grids, condition monitoring and fault diagnosis for power apparatus, multiple-criteria evaluation, and intelligent decision support systems. He is also a Fellow of IET.

**GANG LIU** received the B.Sc., M.Sc., and Ph.D. degrees in electrical engineering from Xi'an Jiaotong University, Xi'an, China, in 1991, 1994, and 1998, respectively. He was a Visiting Scholar with the University of Victoria, Canada, from 2010 to 2011. He is currently an Associate Professor with the School of Electric Power Engineering, South China University of Technology, Guangzhou, China.

**QINGHUA WU** (M'91–SM'97–F'11) received the Ph.D. degree in electrical engineering from Queen's University Belfast (QUB), Belfast, U.K., in 1987, where he was a Research Fellow and subsequently a Senior Research Fellow, from 1987 to 1991. In 1991, he joined the Department of Mathematical Sciences, Loughborough University, U.K., as a Lecturer, where, subsequently, he was appointed as a Senior Lecturer. In 1995, he joined The University of Liverpool, Liverpool, U.K., to take up his appointment as the Chair of Electrical Engineering with the Department of Electrical Engineering and Electronics. He is also with the School of Electric Power Engineering, South China University of Technology, Guangzhou, China, as a Distinguished Professor and the Director of Energy Research Institute. He has authored or coauthored more than 440 technical publications, including 240 journal papers, 20 book chapters, and three research monographs published by Springer. His research interests include nonlinear adaptive control, mathematical morphology, evolutionary computation, power quality, and power system control and operation. He is a Fellow of IET, a Chartered Engineer, and a Fellow of InstMC.